

Toward accurate solvation dynamics of lanthanides and actinides in water using polarizable force fields: from gas-phase energetics to hydration free energies

Aude Marjolin · Christophe Gourlaouen · Carine Clavaguéra · Pengyu Y. Ren · Johnny C. Wu · Nohad Gresh · Jean-Pierre Dognon · Jean-Philip Piquemal

Received: 8 September 2011 / Accepted: 25 February 2012
© Springer-Verlag 2012

Abstract In this contribution, we focused on the use of polarizable force fields to model the structural, energetic, and thermodynamical properties of lanthanides and actinides in water. In a first part, we chose the particular case of the Th(IV) cation to demonstrate the capabilities of the AMOEBA polarizable force field to reproduce both

reference ab initio gas-phase energetics and experimental data including coordination numbers and radial distribution functions. Using such model, we predicted the first polarizable force field estimate of Th(IV) solvation free energy, which accounts for $-1,638$ kcal/mol. In addition, we proposed in a second part of this work a full extension of the SIBFA (Sum of Interaction Between Fragments Ab initio computed) polarizable potential to lanthanides (La(III) and Lu(III)) and to actinides (Th(IV)) in water. We demonstrate its capabilities to reproduce all ab initio contributions as extracted from energy decomposition analysis computations, including many-body charge transfer and discussed its applicability to extended molecular dynamics and its parametrization on high-level post-Hartree–Fock data.

Published as part of the special collection of articles: From quantum mechanics to force fields: new methodologies for the classical simulation of complex systems.

Electronic supplementary material The online version of this article (doi:10.1007/s00214-012-1198-7) contains supplementary material, which is available to authorized users.

A. Marjolin · C. Gourlaouen · J.-P. Dognon (✉)
Laboratoire de Chimie de Coordination des Eléments-f,
CEA, CNRS UMR 3299, CEA Saclay,
91191 Gif-sur Yvette Cedex, France
e-mail: jean-pierre.dognon@cea.fr

A. Marjolin · J.-P. Piquemal (✉)
Laboratoire de Chimie Théorique, UMPC, CNRS UMR 7616,
CC 137 4 Place Jussieu, 75252 Paris Cedex 05, France
e-mail: jpp@lct.jussieu.fr

C. Clavaguéra (✉)
Laboratoire des Mécanismes Réactionnels, Département
de Chimie, Ecole Polytechnique, CNRS,
91128 Palaiseau Cedex, France
e-mail: carine.clavaguera@dcmr.polytechnique.fr

P. Y. Ren · J. C. Wu
Department of Biomedical Engineering, University of Texas
at Austin, Austin, TX 78712-1062, USA

N. Gresh
Laboratoire de Chimie et Biochimie Pharmacochimiques
et Toxicologiques, UMR 8601 CNRS, UFR Biomédicale,
Université Paris Descartes, 45 rue des Saints-Pères,
75270 Paris Cedex 06, France

Keywords Lanthanides · Actinides · Energy decomposition analysis · Polarizable force field · Charge transfer · Hydration free energy

1 Introduction

The fields of interest in lanthanide(III) ions have been extended in the recent years. The main applications cover medical diagnosis (contrast agents in magnetic resonance imaging and luminescent probes for proteins) [1–3], catalysis and organic synthesis [4], organic light-emitting diodes, and nuclear chemistry. The study of the coordination of lanthanide(III) ions and the water exchange in aqueous solutions is of particular importance for the understanding of the chemical processes in which these ions are involved.

Concerning the actinides, the safe management of highly radioactive spent fuel is currently a major challenge for the nuclear energy industry. Fundamental researches

are carried out in such areas as nuclear waste management and nuclear toxicology [5–7]. Consequently, there is a great interest in the knowledge of the chemistry of actinide species. In the reprocessing strategy for nuclear waste, chemical processes are involved; at present, these are based on solvent extraction processes. Such a complex chemical process clearly relies on a delicate balance between the different interactions that govern the system, particularly extractant molecule-cation and water-cation interactions. In this context, the water molecule not only acts as solvent, but it also plays a non-negligible role in complex formation. One of the preliminary steps in understanding the solvent extraction process consists of the study of the lanthanide and actinide cation hydration, and more particularly of the organization of the first coordination sphere around these cations.

Molecular modeling can help to better understand the local complexation properties of the ions and to support the design of new extractant molecules. Classical molecular dynamics (MD) simulations using explicit solvent are essential to investigate statistical and dynamical properties that can be related to rather rare events taking place over hundreds of picoseconds.

In addition, many recent studies highlighted the failure of traditional fixed charge force fields to capture the main physical effects that govern interaction for highly charged ions in polar solvents [8–19].

Consequently, several polarizable models are available in the literature, mainly applied to the study of lanthanide hydration [20–22]. It was stressed [13] that some of them are not general due to the non-transferability of their parameters leading to debatable results including predicted shorter water residence times for the heavier lanthanides than for the lighter ones, in contradiction with well-established experimental data [22]. Moreover, the trends in the water exchange rate are shifted to heavier ions with a maximum at Tb^{3+} instead of Gd^{3+} , in contradiction with the well-known gadolinium break along the lanthanide series [22].

In our previous work on the uranyl ion [23], we pointed out that only an explicit high-level treatment for non-covalent interactions is able to reproduce experimental data. This approach was also pioneered by Hagberg et al. on UO_2^{2+} [11] and Cm^{3+} hydration [12]. The NEMO force field was used including multipolar electrostatic expansions and complete many-body effects, i.e., polarization and charge transfer, but within a rigid molecular framework [24]. The parameters were extracted from a metal–water curve interaction computed at the relativistic multiconfigurational level of theory followed by perturbation theory (CASSCF/CASPT2) and validated by molecular dynamics simulations in water. Two more recent studies were reported on the hydration of actinide ions using polarizable force fields. The EXAFS spectra of a Cf^{3+}

aqueous solution were successfully explained thanks to the design of two specific polarizable intermolecular potentials for eight and nine coordination of the cation and Monte Carlo simulations [16]. Réal et al. performed MD simulations on the Th(IV) in aqueous solution using two different polarizable force fields and including explicit ad hoc Th^{4+} –water charge-transfer term [17]. The influence of the parameter set on the structuration of the first shells was explored, and we will discuss their results later in this paper.

Thanks to high-level electrostatics and full treatment for polarizable effects, MD simulations with AMOEBA [25, 26] were able to reproduce structural and dynamical experimental properties of hydrated mono and divalent metal cations [27–30]. In our previous studies, the AMOEBA polarizable and flexible force field was extended to the lanthanide(III) ions [8–10]. We present here an extension to actinide ions in the same framework.

In addition, we proposed in a second part of this work a full extension of the SIBFA (Sum of Interaction Between Fragments Ab initio computed) [31] approach to trivalent lanthanides and tetravalent actinides. Indeed, the anisotropic polarizable SIBFA force field has been developed to provide an accurate description of divalent metal cations [31–33] in large biological binding sites [34, 35]. SIBFA is able to treat “explicitly” both polarization and charge-transfer contributions and therefore can be used as a reference to understand the many-body effects in large systems.

The parametrization of these two advanced force field requires the use of accurate ab initio reference data. In the case of heavy elements, especially for actinides, relativistic effects and multiconfigurational wave functions are essential to provide reliable reference data. A complete study on the Th(IV) –water dimer has been carried out to state that MRCI level is the best reference to obtain dissociation curves for force field development [36].

We will present first the ab initio methods used for the parameterizations. Then, the second part will be devoted to the extension of AMOEBA to the Th(IV) ion, to the validation of its energetics on Thorium–water clusters and to MD simulations for the determination of structural and thermodynamical data (hydration free energy) in aqueous solution. In the last part, we will present the extension of SIBFA to closed-shell trivalent lanthanides and tetravalent actinides.

2 Procedures

2.1 Interaction energy calculations and levels of ab initio computations

Due to the complex physical and chemical characteristics of lanthanide and actinide systems, high-level ab initio calculations were mandatory, so as to generate reliable data

for the parameterization of the AMOEBA and SIBFA force fields.

For example, in the dissociation of the $[\text{Th}(\text{H}_2\text{O})]^{4+}$ complex, several electronic states which may cross along the minimum energy path are involved. The $[\text{Th}(\text{H}_2\text{O})]^{4+}$ adiabatic dissociation curves computed using a MRCI wave function are given in Fig. 1. At about 2.6 Å, the S_0 state crosses a higher lying S_1 state. An avoided crossing results, which causes strong orbitals, changes. This leads to a net charge transfer that transforms a $\text{Th}^{4+}-\text{H}_2\text{O}$ complex into a $\text{Th}^{3+}-\text{H}_2\text{O}^+$ as the ligand is ionized. In order to compute the required dissociation curve (see curve S_d in Fig. 1) to develop polarizable ab initio-based force fields, a state of the art diabatic representation is mandatory. The full methodology used is described in Gourlaouen et al. [36]. The MRCI calculations [37] were performed with the MOLPRO [38] program package.

The interaction energy is calculated as the difference between the dimer energy and that of the separate fragments for varying $M-\text{O}_w$ distances.

$$E_{\text{int}} = E[M - (\text{OH}_2)]^{m+} - E(M^{m+}) - E(\text{OH}_2)$$

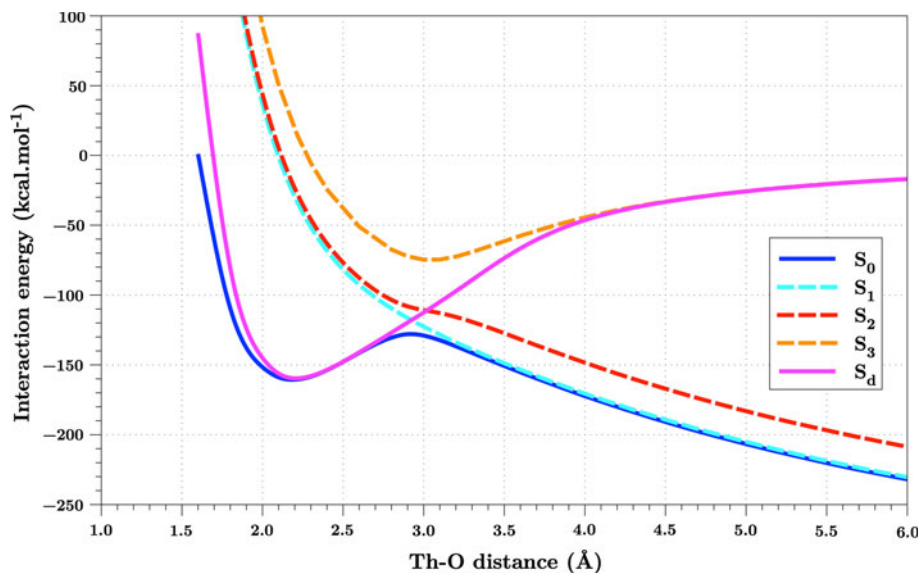
The reference geometry was one in which the water molecule was kept frozen in the experimental geometry (bond length $d_{\text{O-H}} = 0.957$ Å and bond angle $\text{HOH} = 104.5^\circ$ [39]), so that the dimer system interaction energy was calculated in the C_{2v} group. In this manner, the active space used for the multireference calculations consisted for all three systems of the oxygen's highest occupied molecular orbital ($2p_y$) as well as the first virtual orbitals of symmetry 2 of each cation, i.e., two $4f$ orbitals and a $5d$ orbital for La(III), two $5d$ and a $6p$ orbital for Lu(III), and two $5f$ and a $6d$ orbital for Th(IV). Dunning's augmented triple zeta basis set [40] was used on the O and H atoms, while the Stuttgart quasi-

relativistic small-core pseudopotentials and associated basis sets as in MOLPRO's internal library were, respectively, used for La, Lu, and Th. On the other hand, calculations at lower levels of theory (HF and MP2) with both small-core and large-core pseudopotentials were carried out with the Gaussian03 [41] package. The geometry was also kept partially frozen in the experimental geometry except for the Ln/An- O_w bond length. All interaction energy values were corrected of the basis set superposition error (BSSE) by the counterpoise method.

2.2 Energy decomposition analyses

Energy decomposition analyses (EDA) were then carried out to compute the different contributions to the interaction energy of the dimer systems for the parameterization of the AMOEBA and SIBFA force fields. The constrained space orbital variation [42] (CSOV) decomposition at the Hartree-Fock level as implemented in our modified version of HONDO95.3 [43, 44] was carried out for the lanthanide systems, while the restricted variational space [45] (RVS) analysis was carried out with the GAMESS [46] package on the Thorium-water dimer as well as on the different $[M-(\text{OH}_2)_n]^{m+}$ clusters. Both approaches are related to the Morokuma procedure [47] in which the Hartree-Fock interaction energy is separated in four physically meaningful contributions, namely the Coulomb electrostatic energy (ES), the Pauli exchange-repulsion term (REP) (which adds up to give the "frozen core" energy), and POL and CT, which are the polarization energy and the charge-transfer term, respectively; those latter contributions sum up to give the non-frozen energy resulting of the interaction between the two approaching monomers. One advantage of CSOV and RVS is that such methods are able to maintain

Fig. 1 Adiabatic (blue, cyan, red, and orange) and diabatic (magenta) MRCI dissociation curves for $[\text{Th}(\text{H}_2\text{O})]^{4+}$ complex



the correct antisymmetry of the wave function leading to the correct evaluation of polarization and charge-transfer energies [43, 48].

2.3 Sum of interactions between fragments ab initio computed (SIBFA)

SIBFA [31] is a polarizable force field, based on the decomposition of the interaction energy in such a way that its equations are strongly analogous to the EDA description of the energy terms. The interaction energy E_{int} is therefore calculated as follows, and a brief outline of the different contributions is given. However, an extended description of the force field can be found in more detailed works [31, 38, 48].

$$E_{\text{int}} = E_{\text{mtp}^*} + E_{\text{rep}} + E_{\text{pol}^*} + E_{\text{ct}} + E_{\text{disp}}$$

E_{mtp^*} is the Coulomb electrostatic contribution, computed with distributed multipoles (up to quadrupoles) derived from the ab initio HF wave function of the monomer fragments and distributed on the atoms and bond barycenters using the procedure developed by Vigné-Maeder and Claverie [49]. This electrostatic energy includes a correction, the penetration energy, accounting for the overlap of orbitals at short range [50]. Second, E_{rep} is the Pauli short-range repulsion between pairs of parallel spin electrons, given as the sum of the different bond–bond, bond–lone pair, and lone pair–lone pair interactions [51]. E_{pol^*} is the polarization energy contribution, computed with distributed, anisotropic polarizabilities on the individual fragments. The polarizabilities are distributed on the centroids of the localized orbitals (lone pairs and bond barycenters) using the procedure of Garmer and Stevens [52]. The field polarizing each monomer is computed with both the permanent multipoles, already derived for the electrostatic contribution, hence no additional cost of calculation, and the dipoles induced on all the other monomers, in an iterative way. A gaussian function is used for the screening of the polarizing field. In addition to E_{pol^*} , the polarization energy based only on the permanent dipoles, E_{pol} can also be calculated. E_{ct} is the charge-transfer contribution which includes all the effects brought about by the permanent and induced dipoles, therefore leading to a coupling with the polarization term. And last, E_{disp} is the dispersion energy originating from the Van der Waals interaction between induced dipoles. Throughout the different terms, SIBFA takes into accounts many physical properties that are yet inaccessible to most force fields, such as the many-body effects of non-additivity, namely in the polarization energy, in the “explicit” many-body charge-transfer and exchange-repulsion [53] terms as well as anisotropy, accounted for in the short-distance electrostatics, repulsion, dispersion, and the charge-transfer contribution.

For consistency purpose within this work, we propose here a reparametrization of the SIBFA water potential at the aug-cc-pVTZ/HF level based on the reference CSOV values.

2.4 The AMOEBA force field

The AMOEBA (Atomic Multipoles Optimized Energetics for Biomolecular Applications) polarizable force field [25] has already been tested in molecular dynamics (MD) simulations of various systems including metal cation hydration [27–29]. The electrostatic component of the model accounts for permanent charges on each atom as well as dipole and quadrupole moments, all of which are derived from quantum chemical calculations. Furthermore, polarization effects are also explicitly included in this electrostatic component via atomic dipole induction as shown in the equation below:

$$\mu_{i,\alpha}^{\text{ind}} = \alpha_i \left(\sum_j T_{\alpha}^{i,j} M_j + \sum_j T_{\alpha\beta}^{i,j'} \mu_{j,\beta}^{\text{ind}} \right) \quad \text{for } \alpha, \beta = 1, 2, 3$$

with α_i the atomic polarizability of the considered cation, T the usual interaction matrix for sites i and j , and M_j the permanent multipole components. The first term in the equation represents the dipole on site i induced by the permanent multipoles, while the second term corresponds to the dipole on site i induced by the induced dipoles produced at the other atoms. A polarization-damping scheme is used via a smeared charge distribution as proposed by Thole [54]:

$$\rho = \frac{3a}{4\pi} \exp(-au^3)$$

with

$$u = R_{ij}/(\alpha_i\alpha_j)^{1/6}$$

where u is the effective distance between atoms i and j as a function of atomic polarizabilities between them, a is a dimensionless width parameter of the smeared charge distribution, which controls the strength of damping. This parameter was set to 0.39 for water and monovalent ions; however, the value was adjusted to smaller values in the case of divalent cations such as Ca^{2+} , Mg^{2+} , and Zn^{2+} that need a wider charge distribution. Consequently, the value for Th^{4+} was also adjusted using the procedure described below. Repulsion–dispersion interactions (van der Waals) between pairs of non-bonded atoms are represented by a buffered 14–7 potential.

$$U_{ij}^{\text{buff}} = \epsilon_{ij} \left(\frac{1 + \delta}{\rho_{ij} + \delta} \right)^{n-m} \left(\frac{1 + \gamma}{\rho_{ij}^m + \delta} - 2 \right)$$

where ε_{ij} is the potential well depth. In addition, ρ_{ij} is R_{ij}/R_{ij}^0 where R_{ij} is the separation distance between atoms i and j , and R_{ij}^0 is the minimum energy distance. Following Halgren [55], we used fixed values of $n = 14$, $m = 7$, $\delta = 0.07$, and $\gamma = 0.12$. The polarizable water model as developed by Ren and Ponder [25] is employed in this study, and the values for R_{ij} and ε_{ij} are parametrized for the Th^{4+} cation. If charge transfer is not explicitly taken into account, it is nevertheless implicitly included via the van der Waals parameters that are derived from the ab initio calculations that contain all these effects. [27, 28] Such strategy has been shown to be robust enough to perform accurate cluster [8, 9] and condensed phase simulations [27, 28].

3 Results

3.1 AMOEBA: from gas-phase clusters to free energy

3.1.1 Extending AMOEBA to the Thorium (IV) ion

The parameters for Th^{4+} were derived from the ab initio diabatic dissociation curve of the $[\text{Th}(\text{H}_2\text{O})]^{4+}$ complex obtained at the MCSCF/MRCI level, using Dolg et al. quasi-relativistic effective core potential for Thorium and aug-cc-pVTZ Dunning basis sets for H and O [40]. The $6s$, $6p$ Thorium electrons, and all the valence H_2O electrons were correlated. The dipole polarizability α_{Th} of Th^{4+} was previously determined at 1.143 \AA^3 [56]. The repulsion–dispersion parameters were fitted upon 60 various configurations chosen to sample the potential energy surface by varying the Th–O distance and the orientation of the water molecule, so that $\varepsilon_{\text{Th}} = 2.50 \text{ kcal/mol}$ and $R_{\text{Th}} = 3.90 \text{ \AA}$. In addition, the damping factor “ a ” was adjusted to 0.20 for Th^{4+} , so that the AMOEBA polarization energy matched the CSOV polarization values as much as possible following the procedure detailed in previous studies [27, 28].

3.1.2 Simulation details: from clusters to periodic boundary conditions

In order to be consistent with our previous studies and to examine the effect of periodic boundary conditions on Th(IV) solvation, we performed both cluster and periodic boundary conditions simulations. Molecular dynamics simulations were then performed on the $[\text{Th}(\text{H}_2\text{O})_{214}]^{4+}$ cluster at constant temperature with a Nosé–Hoover [57, 58] thermostat. The Beeman [59] algorithm was used for the propagation of dynamical trajectories. The water–Thorium cluster was confined by spherical boundary

conditions with a van der Waals soft wall characterized by a 12–6 Lennard-Jones potential which was set to a fixed buffer distance of 2.5 \AA outside the specified radius of 15 \AA . This value was optimized after several tests to probe the role of the size of the radius sphere. All molecular dynamics simulations were carried out with the TINKER [60] software package at 298 K with a 1 femtosecond time step, for a total simulated time of 1 ns per trajectory. The data are accumulated from four trajectories. Furthermore, simulations using periodic boundary condition (PBC) were also performed to compare the dynamics of the Th^{4+} solvation with the cluster simulations. The long-range electrostatics was modeled using the smooth Particle-Mesh Ewald [61] summation for atomic multipoles with a cutoff of 7 \AA in real space, and the convergence criterion for induced dipole computation was set to 10^{-6} D . The temperature was maintained at 298 K using the Berendsen [62] weak coupling method. Two systems were studied, one containing 215 water molecules and the Th^{4+} ion to match the cluster conditions, and the other 511 water molecules and the Th^{4+} ion, the unit box having 18.643 and 24.857 \AA side length, respectively.

3.1.3 Validation of the AMOEBA potential on Thorium–water clusters: gas-phase energetics

Total interaction energies are reported in Table 1 for the Th–water clusters with 8, 9, and 10 water molecules. These geometries were chosen as they are the representative of the final condensed phase coordination of Th(IV) in water. We propose to test AMOEBA against 3 different geometries of Th(IV) interacting with 10 water molecules within the first and second shells, respectively: $9 + 1$, $8 + 2$, and 10. Due to the size of the basis set for the initial reference level of the AMOEBA model, we had to restrict ourselves to a slightly smaller basis set, namely cc-pVTZ. The given values are corrected of the BSSE. All geometries were optimized at both the MP2 level and with the AMOEBA force field starting from the same structures. As can be seen from Table 1, the AMOEBA absolute interaction energies are in very good agreement with the MP2 ones and the global error on the interaction energy by comparison with

Table 1 Interaction energies (in kcal/mol) of the Th^{4+} clusters calculated at the MP2 level and with the AMOEBA force field

$[\text{Th}-(\text{H}_2\text{O})_n]^{4+}$	MP2	AMOEBA	% Error
8	−740.04	−749.85	1.3
9	−786.56	−790.31	0.5
10	−819.26	−818.30	−0.1
9 + 1	−832.90	−835.04	0.3
8 + 2	−834.81	−843.29	1.0

MP2 is smaller than 1.5%. It is important to point out that through the geometry optimization steps, the spatial organization of the water molecules around the ion are preserved going from size 8 to size 10. Beyond this essential validation, the force field is also able to reproduce energetic order of clusters of a specific size, i.e., the relative energies for the 8 + 2, 9 + 1, and 10 clusters. The transferability of the Th(IV) parameters is then assumed from gas-phase clusters to condensed phase.

3.1.4 Molecular dynamics structural results: AMOEBA versus experiments

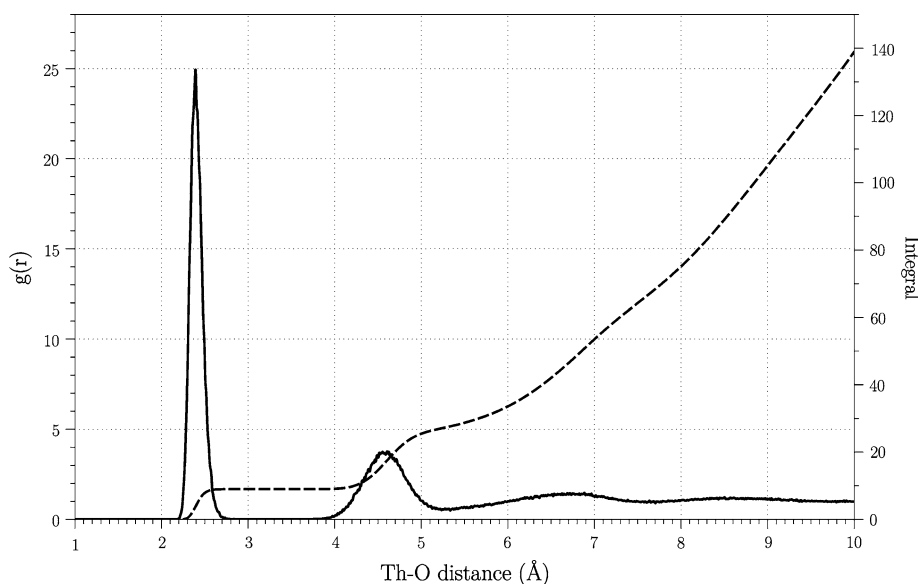
Table 2 presents the main results concerning the structure of the solvation shells around the Th⁴⁺ ion extracted from an analysis of the molecular dynamics trajectories in both cluster and PBC simulations. Since the results are very similar for the four independent trajectories in cluster and the two PBC simulations with different water box sizes, these

Table 2 Molecular dynamics results for the Th⁴⁺–water cluster and from PBC simulations with 215 and 511 water molecules

Properties	MD cluster	MD PBC 215 H ₂ O	MD PBC 511 H ₂ O	Experimental [64]
1st shell				
Average CN	9	9	9	9
Th ⁴⁺ –O _w distance (Å)	2.4	2.41	2.4	2.462
2nd shell				
Number of H ₂ O	18.1	17.7	18.1	18
Th ⁴⁺ –O _w distance (Å)	4.59	4.57	4.63	4.657

structural data are considered to be converged. The average coordination number (CN) in the first sphere was found to be exactly 9.0 from the integration of the narrow first peak observed on the radial distribution function $g(r)$ for Th–O pairs (see Fig. 2). The number of experimental structural investigations of the hydrated Thorium(IV) ion in aqueous solution is limited. Recently, Wilson et al. [63] reported a mean Th⁴⁺–O_w bond distance of 2.46 Å with a coordination number of 10 from wide angle X-ray scattering (WAXS) study in highly concentrated hydrobromic acid. On the other hand, Torapava et al. [64] performed X-ray absorption fine structure LAXS experiments in aqueous solution. As their results have been obtained in lower concentration than the previous authors, they are, therefore, more comparable to our simulations. Consequently, their derived coordination number of 9 and the Th⁴⁺–O_w distance of 2.462 Å have been taken as reference and directly compared with our calculated values. In these conditions, the computed CN of 9.0 is in very good agreement with experiments. No water exchange was observed between the first and the second coordination shells as expected from experimental observations of a residence time of about 20 ns [65]. The maximum peak for the first shell is located at 2.40 Å in good agreement with experimental data. The second sphere is well resolved with a larger peak centered at 4.59 Å, which corresponds to about 18 water molecules. These values match the experimental data [64]. Beyond this distance, no specific geometric arrangement can be pointed out anymore both in cluster and PBC simulations. Figure 3 shows the distribution of the cosines of the angle between the HOH bisector and the Th–O axis for both the first and second shells. A strong radial alignment is obtained with an angle lower than 20° and 25° for the first and second shells, respectively. This confirms the strong influence of the ion on the two first shells.

Fig. 2 Radial distribution function $g(r)$ of Th⁴⁺–O and integrated curve for the Th⁴⁺–water cluster



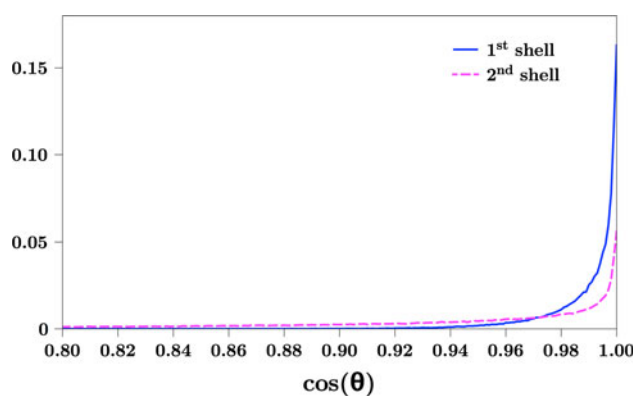


Fig. 3 Probability distribution of the cosines of the tilt angle (between the HOH bisector and the Th–O axis) for the water molecules in the first and second coordination shells in the Th⁴⁺–water cluster case

In a recent study, the solvation of Th(IV) was investigated by molecular dynamics using a polarizable force field [17] with the water geometry constrained to the experimental one. The force fields parameters were adjusted from ab initio calculations, and it was found that the organization of the two first coordination spheres around the cation strongly depends on the parameter sets, especially on the parameters of the charge-transfer term. These simulations led to a coordination number between 8.05 and 8.45, lower than the recent experimental results of Torapova et al. An equilibrium was found between 8- and 9-fold coordination that implies water exchange between the two first coordination spheres. This was never observed experimentally [63].

3.1.5 Hydration free energy of Th(IV)

Molecular dynamics simulations were performed to compute the solvation free energy of Th(IV). Fourteen independent simulations were first performed to “grow” the Th VdW particle by setting the charge and polarizability to zero and gradually varying R as $R(\lambda) = \lambda(R_{\text{final}})$ and ϵ as $\epsilon(\lambda) = \lambda(\epsilon_{\text{final}})$, where $\lambda = (0.0, 0.0001, 0.001, 0.010, 0.1, 0.2, 0.3, 0.4, 0.5, 0.6, 0.7, 0.8, 0.9, 1.0)$. Twenty-one further simulations were then performed to “grow” the +4 charge q of Thorium along with its polarizability α such that $q(\lambda') = \lambda'(q_{\text{final}})$ and $\alpha(\lambda') = \lambda'(\alpha_{\text{final}})$, where $\lambda' = (0.0–1.0$ with a fixed 0.05 increment). Each simulation ran for 500 ps with a 1.0 fs timestep and the same previously described conditions as the periodic boundary conditions computation of the 511 water box. The absolute free energy calculation was carried out on each of the frames saved every 0.1 ps after the first 50 ps equilibration period using the Bennet acceptance ratio [66] (BAR), a free energy calculation method that utilizes forward and reverse perturbations to minimize variance.

Twenty additional simulations of 400 ps each were also performed to sample tighter frames for values of λ' between 0.000 and 0.100 and between 0.900 and 1.000 with 0.01 steps. However, the difference between the preliminary results and the final value is negligible and would not have required any extra steps as the variation of the ΔG value was quite constant between each pair of frames. Conclusively, the accumulated absolute free energy values for the different frames sum up to $-1,635 (\pm 18)$ kcal/mol. Despite a significantly different coordination number, this value is in the range of the available reference (1,458 kcal/mol) value due to David et al. [67] Such value was computed upon EXAFS data using an empirical hydration model based on five basic characteristics of the hydrated ions: crystallographic ionic radius, the coordination number, the cation–oxygen distance (first hydration shell), the number of water molecules in the second hydration shell, and the cation effective charge Z_{eff} . This result is also consistent with the somewhat older results from Marcus [68] who found a value of $-1,391$ kcal/mol with a less refined empirical model also using partial experiment data. Moreover, the values previously obtained with the AMOEBA force field for the divalent cations Ca²⁺, Mg²⁺, and Zn²⁺ [27] (see also Supplementary Informations) show that the relative free energies computed with polarizable molecular dynamics simulations are in line with the experimental literature values, including the one obtained for Th⁴⁺.

3.1.6 Conclusions

The AMOEBA force field has yet again proved to be robust enough to handle dynamic simulations and yield structural and energetics data for cations. However, the non-explicit inclusion of charge transfer in the model can lead to inaccurate modeling in the particular case of lanthanide and actinide systems where water exchange and charge transfer are key phenomena. Being smaller in magnitude compared to polarization, a good percentage of it (namely the two-body part) could be accurately included within AMOEBA's van der Waals term when the many-body charge transfer is not the driving force of the solvation dynamics. Therefore, as Th(IV) retains its first shell water molecules throughout the whole dynamics, the remaining induction contribution (charge transfer) can be said to be included in the Van der Waals term as a result of matching the total binding energy of AMOEBA to that of quantum mechanics, regardless of the different individual contributions. While the present study does not call for the explicit treatment for charge transfer, other systems will require the computation of both induction terms so as to capture the overall many-body effects, and hence, a project aiming to include an explicit contribution of the charge transfer in the

AMOEBa force field is underway. Nonetheless, we still aimed to investigate the variation of the charge-transfer energy in the Thorium–water clusters as well as in the Lanthanum– and lutetium–water clusters, which are, respectively, the first and last of the lanthanide series using the SIBFA force field as described in the next section.

3.2 Extending the SIBFA force field to lanthanides and actinides

As we have seen, in SIBFA, the intermolecular interaction is expressed under the form of distinct contributions. Each contribution is calibrated in order to closely reproduce its ab initio counterpart as obtained from energy decomposition analyses on monoligated ($M\text{-H}_2\text{O}$)ⁿ⁺ metal cation–water complexes.

3.2.1 Interaction energies

The aim of working at different levels of calculation was to determine whether the HF/large-core pseudopotential/aug-cc-pVTZ level as in the energy decomposition scheme and consequently for the parameterization of the SIBFA force field was relevant. The comparable profiles of the interaction energy curves in the considered range for the parameterization (1.5–3.5 Å) in all cases show that the chosen level can safely be used for the energy decomposition within the CSOV and RVS frameworks for the development of the SIBFA potential (Fig. 4). The difference between the post-HF and HF energies at the minimum of the curves is the missing correlation energy in the Hartree–Fock approach and can be partially recovered in the force field through the dispersion energy as a rough approximation. Namely, this correlation energy accounts for nearly 10% of the total energy at MP2 level and is due to the high number of electrons in the lanthanides and actinides that are not taken into account explicitly in the large-core pseudopotentials. Therefore, the correlation calculated at the MP2 level recovers the missing energy. The BSSE is negligible in all cases (less than 2% in the considered range) at the HF level.

3.2.2 Energy decomposition analyses

Detailed numerical values about EDA contributions can be found in several Tables in the Supplementary Information section.

Table 3 shows the energy decomposition analysis around the optimized distances of 2.4, 2.1, and 2.2 Å, respectively, for the $[\text{La-OH}_2]^{3+}$, $[\text{Lu-OH}_2]^{3+}$ and $[\text{Th-OH}_2]^{4+}$ dimers. All energies are given in kcal/mol. In both cases of the lanthanide cations bearing the same +3 charge, the contribution of the first-order energies amount to the

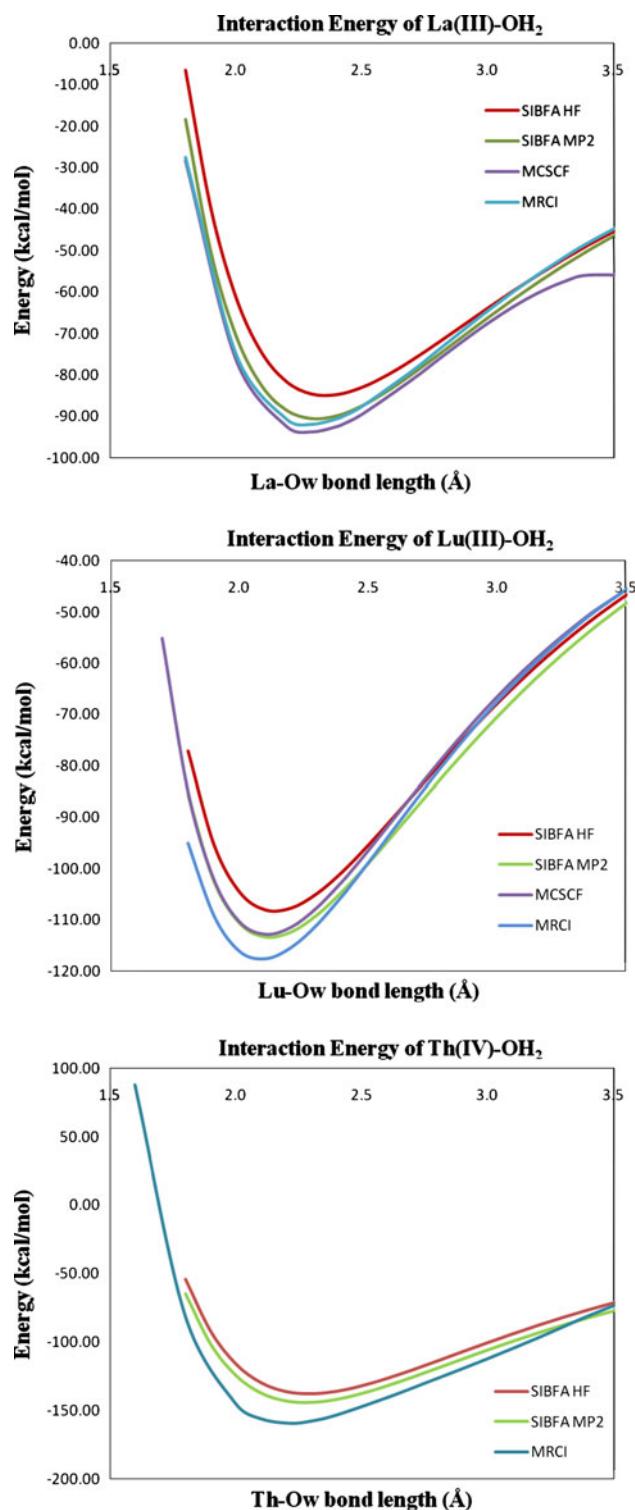


Fig. 4 Ab initio interaction energy curves at different levels of calculation for all three dimers using the procedure described in Sect. 1

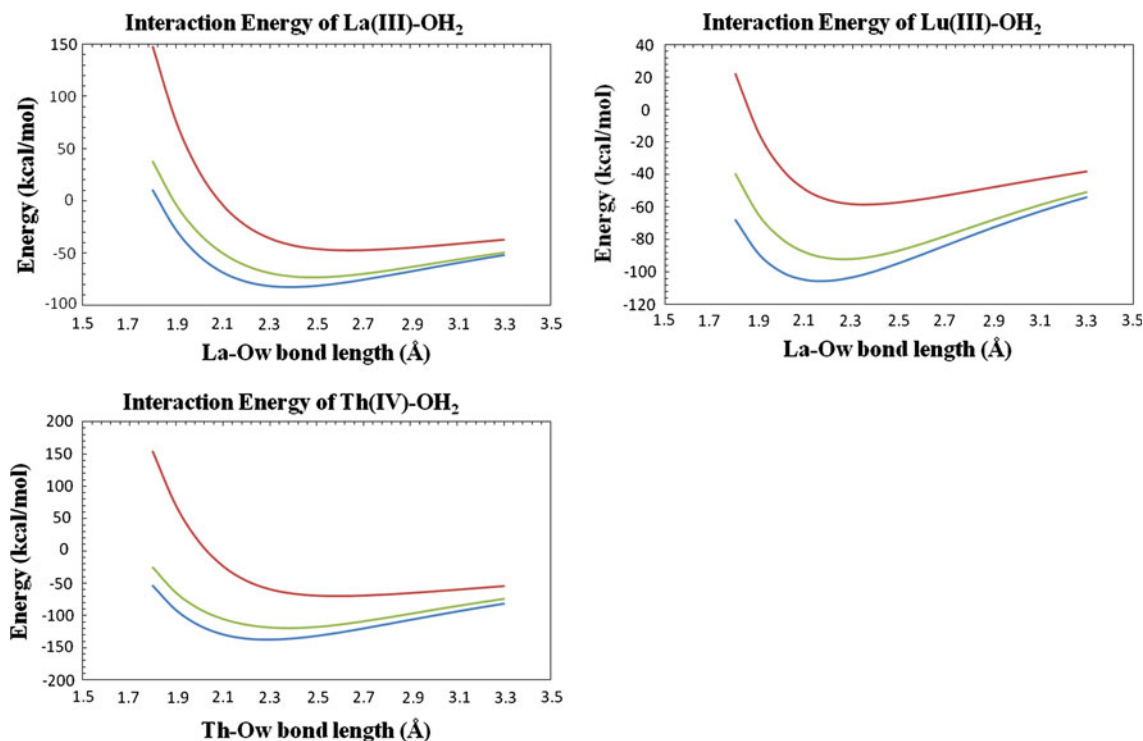
same value even though the separate energies of electrostatics (ES) and exchange repulsion (REP) are significantly higher in the Lutetium–water dimer. This is of course due

Table 3 The different energy contributions, in kcal/mol, as given by the CSOV and RVS decomposition at the HF level, as well as the global interaction energy (E_{int}) at the equilibrium distances for the $[\text{La}-\text{OH}_2]^{3+}$, $[\text{Lu}-\text{OH}_2]^{3+}$, and the $[\text{Th}-\text{OH}_2]^{4+}$ dimers

Dimer	ES	REP	E1	POL	CT	E_{int}
$[\text{La}-\text{OH}_2]^{3+}$	-67.56	35.50	-32.07	-40.17	-10.40	-82.64
$[\text{Lu}-\text{OH}_2]^{3+}$	-85.43	52.84	-32.59	-55.29	-16.92	-104.79
$[\text{Th}-\text{OH}_2]^{4+}$	-102.55	83.13	-19.42	-92.80	-30.45	-145.26

to the increased number of electrons from the Lanthanum $4f^0$ configuration to the completely filled $4f^{14}$ shell of Lutetium, even though they are not accounted for explicitly in the pseudopotentials. However, both the polarization energy (POL) and the charge transfer (CT) are higher in the Lutetium system and are therefore responsible for the global increase in the interaction energy value, of 22.15 kcal/mol, from $[\text{La}-\text{OH}_2]^{3+}$ to $[\text{Lu}-\text{OH}_2]^{3+}$. In the case of the $[\text{Th}-\text{OH}_2]^{4+}$ dimer, the Coulomb energy is as expected, significantly higher than in the trivalent systems and so is the repulsion energy, thus resulting in a decreased first-order energy (E1) with respect to the Lanthanum and Lutetium systems. Conversely, both the polarization energy and charge-transfer contributions have increased, with POL accounting for more than 60% of the interaction energy of the Thorium system and $\sim 50 \pm 2\%$ in the case of the two lanthanide systems. It is clearly shown here that, despite the high positive charge of the cations, the main contribution to the interaction energy is the polarization

term when compared to E1. In addition to polarization, the charge-transfer term appears to be clearly non-negligible and therefore hints to more covalent interactions in such systems. Therefore, the degree of covalency in those bonds is linked to the second-order energies and will be clearly dependent on the type of cation (and on the involved orbitals and presence and number of f electrons in the system). As a result, we pointed out that neglecting either one or the other of the second-order contributions will induce a shift in the equilibrium distance and corresponding energy as shown in Fig. 5 for lanthanide and actinide systems. It is important to note that the use of a EDA formalism such as CSOV is important for such ab initio decomposition. Indeed, CSOV generates consistent polarization data as the HF wave functions are kept strictly antisymmetric. That way, here, we do not have any over-estimation of polarization/charge transfer due to such lack of antisymmetry (i.e., exchange polarization is included, see references 40 and 45 for details). In any case, these

**Fig. 5** Ab initio energy curves excluding either the charge-transfer term (green) or the polarization energy (red) as compared to the interaction energy (blue) for all three dimers

results clearly rise key issue toward force fields development that should either: (a) embody an explicit functional form for charge transfer or (b) at least follow a consistent parametrization strategy to incorporate charge transfer in van der Waals based on EDA as some of us proposed [27].

3.2.3 Extension of the SIBFA potential to lanthanides and actinides

At the end of this work, a full SIBFA potential was obtained for all three considered cations, with a very good description of each energy contribution by the force field with respect to the reference data as shown in Fig. 6 for Th(IV) –(La(III) and Lu(III) Figures are available as SI: see Figures SI7 and SI8). It can be noted here that SIBFA's first handling of trivalent and tetravalent cations shows a very good reproduction of the different ab initio contribution curves. Moreover, concerning the electrostatic contribution, the inclusion of a correction of the quantum penetration energy through an overlap term prevented any divergence at short range. Also, all pair approximations made for the repulsion term are entirely transferable up to the heavy elements as previously shown for the Pb(II) cation [69], with correct behavior of the SIBFA force field at both short- and long range. Concerning the second-order energies, results are satisfactory. At very short distances, the SIBFA polarization energy diverges from the CSOV curve, indicating that the damping is not sufficient since the

CSOV polarization term grows more rapidly than its SIBFA counterpart as the Ln/An–O_w distance decreases. Such behavior which is nevertheless not critical will be avoided in a near future through the use of a Gaussian electrostatic potential based on density fitting such as the Gaussian electrostatic model (GEM) [70]. This approach which is being implemented within SIBFA [71] will allow for a better reproduction of the short-range curvature of the polarization and thus avoid the polarization catastrophe. Lastly, the charge transfer gives satisfying agreement with ab initio, namely around the optimized distance with a slight divergence however at very short and very long distances. Overall, the agreement between SIBFA's global interaction energy with the ab initio value obtained from the quantum EDA is also very satisfactory (Fig. 7) and indicates SIBFA's ability to reproduce the ab initio interaction energy for trivalent lanthanide–water and tetravalent actinide–water dimers.

3.2.4 Transferability of the potential

The transferability of the different parameters optimized for the dimer systems was tested for several [Ln–(OH₂)_n]³⁺ and [Th–(OH₂)_n]⁴⁺ clusters, with *n* = 4, 6, 8, and 9 (structures for which RVS computations were technically possible). The geometries of the tetra-coordinated clusters were optimized at the HF level using aug-cc-pVTZ basis sets for the water molecules and a small-core

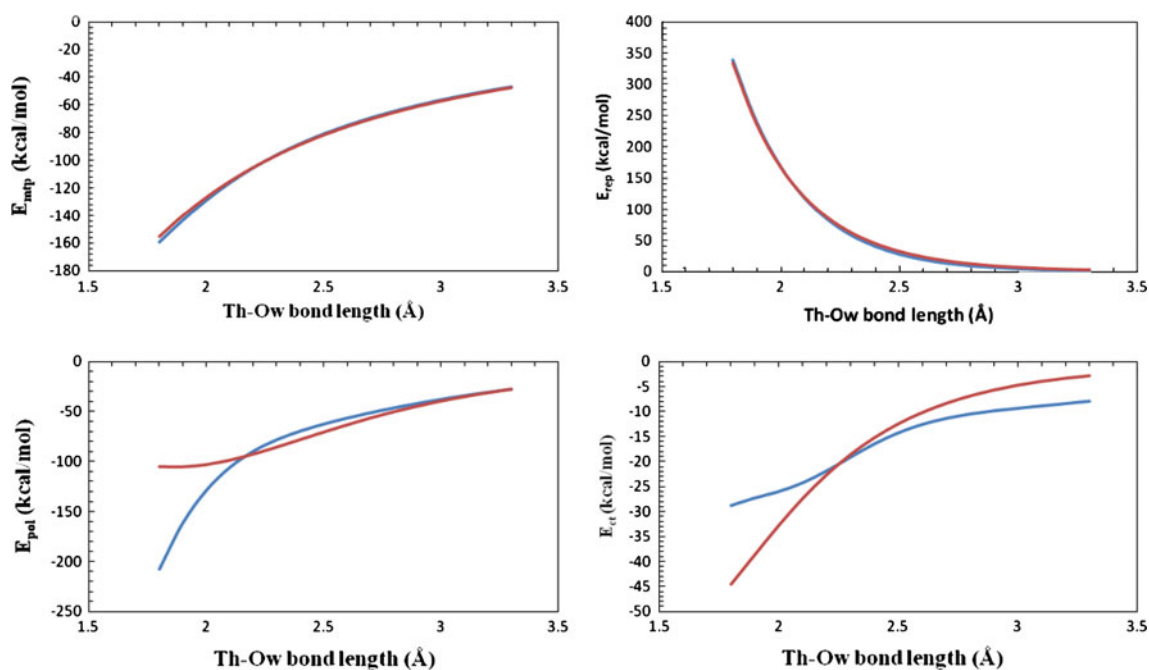


Fig. 6 CSOV (blue) versus SIBFA (red) electrostatic (top left), repulsion (top right), polarization (bottom left), and charge-transfer (bottom right) energies as a function of the Th–O_w distance in Th(IV)–OH₂

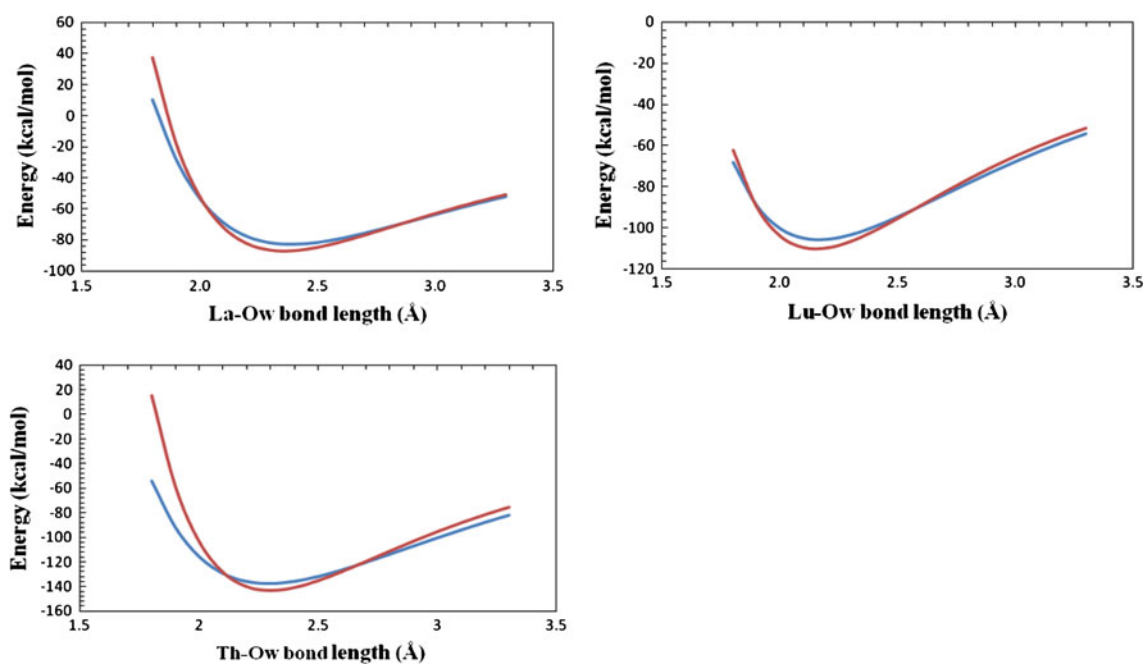


Fig. 7 CSOV (blue) versus SIBFA (red) total interaction energies as a function of metal M–O_w distances in M(*n*+)-OH₂ at the HF level

pseudopotential for Th. The structure of the complex with eight-coordinated water molecules is square antiprismatic (SAP), while the structure of the complex with nine water molecules is tricapped trigonal prismatic (TTP). As SIBFA uses a rigid fragment approximation, initial geometries were projected within the usual SIBFA model water internal geometry. The Ln/An–O_w distances only were then fixed at three different distances around the optimized bond length. The hexa-coordinated structures however were standard, symmetrical complexes in which only the Ln/An–O_w distances were varied. EDA were then carried out with the GAMESS software to yield the different contributions to the interaction energy of the systems. We have to point out here that while the RVS scheme worked fine for all tetracoordinated clusters, we have not been able to obtain a converged decomposition in the case of the different hexacoordinated clusters. The energy decomposition was therefore carried out in the Kitaura–Morokuma (KM) framework, with as a result, a global second-order energy that was compared to the SIBFA $E_2 = E_{\text{int}} - E_{\text{mtp}} - E_{\text{rep}}$ values instead of the separate polarization and charge-transfer contributions. The comparable energies namely around the optimized distances for each of the tetra- and hexa-coordinated clusters account for the transferability of the parameters, with less than 2% error in the global interaction energy around the considered distances.

Lastly, the parameters were tested on more relevant structures of eight- and ninefold coordination for all three systems. However, due to computational limits, only the interaction energy at the Hartree–Fock level calculated

with the Gaussian program was used for comparison against the SIBFA interaction energy on the same structures. Once again, the error is kept under the aforementioned 2% in all three Lanthanum, Lutetium, and Thorium systems as shown in Tables 4, 5, 6. We have therefore obtained a fully transferable, polarizable force field, including charge transfer, for trivalent closed-shell lanthanide and tetravalent actinide cations.

3.2.5 The issue of dispersion: toward correlated molecular dynamics

The last contribution taken into account by the SIBFA force field is the dispersion energy, i.e., the energy arising from the dynamically induced dipoles. Per se, this contribution cannot be derived from a Hartree–Fock energy decomposition analysis, and therefore, it has been taken in this study as the difference between an MP2 dissociation curve and the HF curve used to parameterize the SIBFA force field. Despite the approximate fit of the SIBFA E_{disp} component on the $\Delta(\text{MP2-HF})$ curve, the overall MP2 interaction energy curve matches that obtained with the SIBFA potential corrected with the estimated dispersion component from the fit, referred to as SIBFA + d, as it can be seen in Supplementary Informations (SI: Figure 9). While the results for the cation-monoaqua systems feature less than 5% error, the extension to the different clusters is still out of reach because the nature of the dispersion energy is not fully accounted for in the $\Delta(\text{MP2-HF})$ approximation as correlation is not restricted to the sole

Table 4 Interaction energies in kcal/mol of the $[\text{La}-(\text{OH}_2)_n]^{3+}$ clusters as calculated at the Hartree–Fock (HF) level and with the SIBFA force field for several ion–water distances

<i>n</i>	<i>d</i> (La–O _w) (Å)	HF	SIBFA	Δ	% Error
4	2.3	–268.66	–263.38	–5.28	2.0
	2.4	–279.69	–277.45	–2.24	0.8
	2.5	–281.39	–280.13	–1.26	0.5
6	2.1	–189.21	–166.13	–23.08	12.2
	2.2	–277.58	–264.90	–12.68	4.6
	2.3	–330.42	–323.53	–6.89	2.2
	2.4	–358.71	–354.76	–3.95	1.1
	2.5	–370.24	–367.49	–2.75	0.7
8	2.60	–419.71	–415.11	–4.6	1.1
9	2.63	–451.24	–447.5	–3.73	0.8

The relative difference Δ between each pair of values is given as well as the corresponding percentage error

Table 5 Interaction energies in kcal/mol of the $[\text{Lu}-(\text{OH}_2)_n]^{3+}$ clusters as calculated at the Hartree–Fock (HF) level and with the SIBFA force field for several ion–water distances

<i>n</i>	<i>d</i> (Lu–O _w) (Å)	HF	SIBFA	Δ	% Error
4	2.2	–351.36	–344.07	–7.29	2.1
	2.3	–350.65	–347.05	–3.60	1.0
	2.4	–342.44	–340.00	–2.44	0.7
6	2.1	–419.09	–389.94	–29.15	7.0
	2.2	–448.29	–432.33	–15.96	3.6
	2.3	–457.28	–448.88	–8.40	1.8
	2.4	–453.47	–448.63	–4.84	1.1
	2.5	–441.26	–437.78	–3.48	0.8
8	2.42	–505.72	–496.18	–9.54	1.89
9	2.43	–536.21	–533.26	–2.95	0.55

The relative difference Δ between each pair of values is given as well as the corresponding percentage error

dispersion term. Indeed, preliminary calculations have shown that the parameters derived for dispersion in SIBFA do not exhibit the same transferability as that obtained for the other contributions. A means of accessing a more physically meaningful dispersion contribution is through post-HF EDA, such as correlated CSOV or by performing EDA on correlated energy curves. This however implies intensive studies so as to determine which functional is more appropriate to each of the investigated systems while remaining cautious on the ability of the density functional theory to assess lanthanide and actinide systems.

4 Conclusion

The parameterization of the SIBFA force field for the first and last cations of the lanthanide series and the

Table 6 Interaction energies in kcal/mol of the $[\text{Th}-(\text{OH}_2)_n]^{4+}$ clusters as calculated at the Hartree–Fock (HF) level and with the SIBFA force field for several ion–water distances

<i>n</i>	<i>d</i> (Th–O _w) (Å)	HF	SIBFA	Δ	% Error
4	2.3	–469.22	–470.13	0.91	–0.2
	2.4	–470.46	–477.44	6.98	–1.5
	2.5	–462.10	–469.25	7.15	–1.6
6	2.1	–475.89	–390.34	–85.55	18.0
	2.2	–555.23	–518.73	–36.5	6.6
	2.3	–598.21	–588.47	–9.74	1.6
	2.4	–615.69	–618.50	2.81	–0.5
	2.5	–615.57	–622.26	6.69	–1.1
8	2.50	–693.80	–701.81	8.01	–1.2
9	2.56	–735.70	–743.22	7.52	–1.0

The relative difference Δ between each pair of values is given as well as the corresponding percentage error

closed-shell Thorium(IV) cation was undertaken. It was found that SIBFA, which includes many-body charge transfer, is capable of handling heavy elements from dimers to ninefold coordinated hydrated complexes with around 2% error with respect to the ab initio Hartree–Fock interaction energy. Furthermore, the fact that the force field is based on EDA has led us to investigate the separate contributions to the interaction energy of the considered dimers. The sizeable values of the polarization and charge-transfer energies secures the idea that only a polarizable force field including charge transfer can be used to correctly model lanthanide and actinide systems. Nevertheless, through its careful parametrization on the Th(IV)–water dimer and without including any experimental data, the AMOEBA force field leads to very accurate results. The transferability of the parameters has been demonstrated since the force field was able to reproduce gas-phase reference energetic, structural, and thermodynamical experimental quantities, including Th(IV) solvation free energies. Such results are encouraging and should lead us to improved modeling of lanthanides and actinides within complex environments beyond solvation. To conclude, based on the SIBFA results, explicit charge transfer will be added to AMOEBA as full SIBFA cluster MD simulations will be undergone. Moreover, as our approaches are not limited to treat closed-shell systems, [32] future work will also deal with open-shell actinides systems (Marjolin et al. in preparation).

Acknowledgments Two of the authors, C. G. and J.-P. D., thank the direction of simulation and experimental tools of the CEA nuclear energy division CEA/DEN/RBPCH for financial support. This work was granted access to the HPC resources of [CCRT/CINES/IDRIS] under the allocation x2011086146 made by GENCI (Grand Equipement National de Calcul Intensif).

References

1. Merbach AE, Toth E (2001) The chemistry of contrast agents in medical magnetic resonance imaging. Wiley, Chichester
2. Nicholas LK, Long NJ (2006) Chem Soc Rev 35:557
3. Moore EG, Samuel APS, Raymond KN (2009) Acc Chem Res 42:542
4. Hou ZM, Wakatsuki Y (2002) Coord Chem Rev 231:1
5. Silva R, Nitsche H (1995) Radiochim Acta 70:377
6. Grenthe I, Fuger J, Konings R, Lemire R, Muller A, Nguyen-Trung C, Wanner H (1992) In: Wanner H, Forest I (eds) Chemical thermodynamics of Uranium. North-Holland, Amsterdam
7. Nash KL, Madic C, Mathur JN (2006) Actinide separation science and technology. In: Morss LR, Edelstein NM, Fuger J (eds) The chemistry of the actinide and transactinide elements. Springer, Dordrecht
8. Clavaguéra C, Calvo F, Dognon J-P (2006) J Chem Phys 124:074505
9. Clavaguéra C, Sansot E, Calvo F, Dognon J-P (2006) J Phys Chem B 110:12848
10. Clavaguéra C, Pollet R, Soudan JM, Brenner V, Dognon J-P (2005) J Phys Chem B 109:7614
11. Hagberg D, Karlström G, Roos BJ, Gagliardi L (2005) J Am Chem Soc 127:14250
12. Hagberg D, Bednarz E, Edelstein NM, Gagliardi L (2007) J Am Chem Soc 129:14136
13. Villa A, Hess B, Saint-Martin H (2009) J Phys Chem B 113:7270
14. Duvaill M, Vitorge P, Spezia R (2009) J Chem Phys 130:104501
15. Beuchat C, Hagberg D, Spezia R, Gagliardi L (2010) J Phys Chem B 114:15590
16. Galbis E, Hernández-Cobos J, den Auwer C, Le Naour C, Guillaumont D, Simoni E, Pappalardo RR, Sánchez ME (2010) Angew Chem Int Ed 49:3811
17. Réal F, Trumm M, Vallet V, Schimmelpfennig B, Masella M, Flament J-P (2010) J Phys Chem B 114:15913
18. Duvaill M, Spezia R, Vitorge P (2008) Chem Phys Chem 9:693
19. Duvaill M, Martelli F, Vitorge P, Spezia R (2011) J Chem Phys 135:044503
20. Kowall Th, Foglia F, Helm K, Merbach AE (1995) J Am Chem Soc 117:13790
21. D'Angelo P, Zitolo A, Migliorati V, Chillemi G, Duvaill M, Vitorge P, Abadie S, Spezia R (2011) Inorg Chem 50:4572
22. Helm L, Merbach AE (2005) Chem Rev 105:1923
23. Clavaguéra-Sarrio C, Brenner V, Hoyau S, Marsden CJ, Millié P, Dognon J-P (2003) J Phys Chem B 107:3051
24. Engkvist O, Åstrand PO, Karlström G (2000) Chem Rev 100:4087
25. Ren P, Ponder JW (2003) J Phys Chem B 107:5933
26. Shi Y, Wu C, Ponder JW, Ren P (2011) J Comput Chem 32:967
27. Wu J, Piquemal J-P, Chaudret R, Reinhardt P, Ren P (2010) J Chem Theory Comput 6:2059
28. Piquemal J-P, Perera L, Cisneros GA, Ren P, Pedersen LG, Darden TA (2006) J Chem Phys 125:054511
29. Jiao D, King C, Grossfield A, Darden TA, Ren P (2006) J Phys Chem B 110:18553
30. Grossfield A, Ren P, Ponder JW (2003) J Am Chem Soc 125:15671
31. Gresh N, Cisneros GA, Darden TA, Piquemal J-P (2007) J Chem Theory Comput 3:1960
32. Piquemal J-P, Williams-Hubbard B, Fey N, Deeth RJ, Gresh N, Giessner-Prettre C (2003) J Comput Chem 24:1963
33. Gresh N, Piquemal J-P, Krauss M (2005) J Comput Chem 26:1113
34. Roux C, Gresh N, Perera L, Piquemal J-P, Salmon L (2007) J Comput Chem 28:938
35. Jenkins LMM, Hara T, Durell SR, Hayashi R, Inman JK, Piquemal J-P, Gresh N, Appella E (2007) J Am Chem Soc 129:11067
36. Gourlaouen C, Clavaguéra C, Piquemal J-P, Dognon J-P (2012) submitted
37. Simah D, Hartke B, Werner H-J (1999) J Chem Phys 111:4523
38. Werner HJ, Knowles PJ with contributions from Almlof J, Amos RD, Bernhardsson A, Berning A, Cooper DL, Deegan MJO, Dobbyn AJ, Eckert F, Hampel C, Lindh R, Lloyd AW, Meyer W, Mura ME, Nicklass A, Peterson K, Pitzer R, Pulay P, Rauhut G, Schutz M, Stoll H, Stone AJ, Taylor PR, Thorsteinsson T (2008) Molpro, version 2008.1. University of Stuttgart and Birmingham, Germany and Great Britain
39. Benedict WS, Gailar N, Plyler EK (1956) J Chem Phys 24:1139
40. Dunning TH Jr (1989) J Chem Phys 90:1007
41. Frisch MJ, Trucks GW, Schlegel HB, Scuseria GE, Robb MA, Cheeseman JR, Montgomery JJA, Vreven T, Kudin KN, Burant JC, Millam JM, Iyengar SS, Tomasi J, Barone V, Mennucci B, Cossi M, Scalmani G, Rega N, Petersson GA, Nakatsuji H, Hada M, Ehara M, Toyota K, Fukuda R, Hasegawa J, Ishida M, Nakajima T, Honda Y, Kitao O, Nakai H, Klene M, Li X, Knox JE, Hratchian HP, Cross JB, Bakken V, Adamo C, Jaramillo J, Gomperts R, Stratmann RE, Yazyev O, Austin AJ, Cammi R, Pomelli C, Ochterski JW, Ayala PY, Morokuma K, Voth GA, Salvador P, Dannenberg JJ, Zakrzewski VG, Dapprich S, Daniels AD, Strain MC, Farkas O, Malick DK, Rabuck AD, Raghavachari K, Foresman JB, Ortiz JV, Cui Q, Baboul AG, Clifford S, Cioslowski J, Stefanov BB, Liu G, Liashenko A, Piskorz P, Komaromi I, Martin RL, Fox DJ, Keith T, Al-Laham MA, Peng CY, Nanayakkara A, Challacombe M, Gill PMW, Johnson B, Chen W, Wong MW, Gonzalez C, Pople JA (2009) Gaussian 09. Gaussian Inc., Wallingford, CT
42. Bagus PS, Hermann K, Bauschlicher CW Jr (1984) J Chem Phys 81:1966
43. Piquemal J-P, Marquez A, Parisel O, Giessner-Prettre C (2005) J Comput Chem 26:1052
44. Dupuis M, Marquez A, Davidson ER HONDO95.3, Quantum Chemistry Program Exchange (QCPE). Indiana University, Bloomington, IN 47405
45. Stevens WJ, Fink W (1987) Chem Phys Lett 139:15–22
46. Schmidt MW, Baldrige KK, Boatz JA, Elbert ST, Gordon MS, Jensen JH, Koseki S, Matsunaga N, Nguyen KA, Su S, Windus TL, Dupuis M, Montgomery JA Jr (1993) J Comput Chem 14:1347
47. Kitaura K, Morokuma K (1976) Int J Quantum Chem 10:325
48. Cisneros GA, Darden TA, Gresh N, Reinhardt P, Parisel P, Pilmé J, Piquemal J-P (2009) In: York DM, Lee T-S (eds) Multi-scale quantum models for biocatalysis: modern techniques and applications, for the book series: challenges and advances in computational chemistry and physics. Springer, Berlin, pp 137–172
49. Vigné-Maeder F, Claverie P (1988) J Chem Phys 88:4934
50. Piquemal J-P, Gresh N, Giessner-Prettre C (2003) J Phys Chem A 107:10353
51. Piquemal J-P, Chevreau H, Gresh N (2007) J Chem Theory Comput 3:824
52. Garmer DR, Stevens WJ (1989) J Chem Phys 93:8263
53. Chaudret R, Gresh N, Parisel O, Piquemal J-P (2011) J Comput Chem 7:618
54. Tholé BT (1981) Chem Phys 59:341
55. Halgren TA (1992) J Am Chem Soc 114:7827
56. Réal F, Vallet V, Clavaguéra C, Dognon JP (2008) Phys Rev A 78:052502
57. Nose S (1984) J Chem Phys 81:511–519
58. Hoover WG (1985) Phys Rev A 31:1695
59. Beeman D (1976) J Comp Phys 20:130

60. Ponder JW (2009) TINKER: software tools for molecular design, version 6.2. Washington University School of Medicine, Saint Louis
61. Essmann U, Perera L, Berkowitz ML, Darden T, Lee L, Pedersen LG (1995) *J Chem Phys* 101:8577
62. Berendsen HJC, Postma JPM, van Gunsteren WF, DiNola A, Haak JR (1984) *J Chem Phys* 81:3684
63. Wilson RE, Skanthakumar S, Burns PC, Soderholm L (2007) *Angew Chem* 119:8189
64. Torapava N, Persson I, Eriksson L, Lundberg D (2009) *Inorg Chem* 48:11712
65. Farkas I, Grenthe IJ (2000) *Phys Chem A* 104:1201
66. Bennett CH (1976) *J Comput Phys* 22:245
67. David FH, Vokhmin V (2003) *New J Chem* 27:1627
68. Marcus YA (1994) *Biophys Chem* 51:111
69. Devereux M, van Severen M-C, Parisel O, Piquemal J-P, Gresh N (2011) *J Chem Theory Comput* 7:138
70. Piquemal J-P, Cisneros GA, Reinhardt P, Gresh N, Darden TA (2006) *J Chem Phys* 124:104101
71. Chaudret R, Gresh N, Darden TA, Parisel O, Cisneros GA, Piquemal J-P (2011) *J Chem Phys* 2012 (in press)